Supported Catalysts Hot Paper

Deutsche Ausgabe: DOI: 10.1002/ange.201601661
Internationale Ausgabe: DOI: 10.1002/anie.201601661

# $CO_2$ Hydrogenation over Oxide-Supported PtCo Catalysts: The Role of the Oxide Support in Determining the Product Selectivity

*Shyam Kattel[+], Weiting Yu[+], Xiaofang Yang, Binhang Yan, Yanqiang Huang, Weiming Wan, Ping Liu,* and Jingguang G. Chen**

***Abstract:*** *By simply changing the oxide support, the selectivity of a metal–oxide catalysts can be tuned. For the $CO_2$ hydrogenation over PtCo bimetallic catalysts supported on different reducible oxides ($CeO_2$, $ZrO_2$, and $TiO_2$), replacing a $TiO_2$ support by $CeO_2$ or $ZrO_2$ selectively strengthens the binding of C,O-bound and O-bound species at the PtCo–oxide interface, leading to a different product selectivity. These results reveal mechanistic insights into how the catalytic performance of metal–oxide catalysts can be fine-tuned.*

The performance of a catalyst depends strongly on its binding properties. According to the Sabatier principle,[1] a good catalyst should bind the reaction intermediates strongly enough to activate the reactants and weakly enough to allow for product desorption. Various approaches have been applied to optimize the structure of a catalyst and to tune the binding properties and therefore the catalytic activity. Typically, the binding energies of various adsorbates vary linearly with changing the local structure of a catalyst or its composition to form alloys.[2] As a result, the catalytic activity towards a reaction can be enhanced by accelerating the activity-limiting steps along the reaction pathway;[3] however, it makes the control of product selectivity more difficult, which often requires the non-linear tuning of the binding energies of different adsorbates.

Herein, we report a possibility to move away from the linear scaling principle by taking advantage of strong metal–oxide interactions to selectively modify the binding energies of particular adsorbates. The special synergy between metals and oxides can introduce large electronic perturbations in the metals,[4] provide heterogeneous sites,[3d,5] or induce variations in the structure or phase of the supported metal particles,[6] which directly affect the bonding properties and correspondingly the catalyst performance. Carbon dioxide ($CO_2$) hydrogenation on PtCo bimetallic catalysts supported on different reducible oxides ($CeO_2$, $ZrO_2$, and $TiO_2$) was taken as a case study. When different oxide supports were used, the binding of the metal–oxide interface to various reaction intermediates changed; however, the response was very different depending on the species. This non-linear response enables the significant tuning of the selectivity of metal oxide catalysts whereas the overall reactivity was much less affected. A combination of ambient pressure X-ray photoelectron spectroscopy (AP-XPS) and density functional theory (DFT) calculations for the model catalysts and transmission electron microscopy (TEM), Fourier transform infrared (FTIR) spectroscopy, diffuse reflectance infrared Fourier transform spectroscopy (DRIFTS), and extended X-ray absorption fine structure (EXAFS) analysis for the corresponding powder catalysts provided insight into how the performance of metal–oxide catalysts can be fine-tuned.

The catalytic conversion of $CO_2$ into methane ($CH_4$),[6c,7] methanol ($CH_3OH$),[3d,8] and carbon monoxide (CO)[6c,9] has gained tremendous interest in recent years. The generation of $CH_4$ from $CO_2$ is not profitable considering the large shale gas reserves and its low volumetric energy density. $CH_3OH$ synthesis has been well studied, but the current market demand for $CH_3OH$ would only reduce the global $CO_2$ emission by 0.1 % if all $CH_3OH$ was produced from $CO_2$.[10] Therefore, one of the most desirable routes for $CO_2$ conversion is the production of CO, the feedstock for the Fischer–Tropsch process to produce chemicals and fuels. Achieving a high selectivity to the desired CO product rather than $CH_4$ and $CH_3OH$ is critical, yet challenging in practical applications.

Metal-based catalysts on oxide supports enable the conversion of $CO_2$. Copper-based catalysts have been found to covert $CO_2$ and hydrogen into $CH_3OH$,[8a,11] whereas platinum-, gold-, and silver-based catalysts promote the conversion of $CO_2$ into CO.[12] Herein, we demonstrate how the selectivity of PtCo catalysts can be fine-tuned by using oxide supports. Whereas a $PtCo/TiO_2$ catalyst effectively converts $CO_2$ and $H_2$ into CO, $PtCo/CeO_2$ and $PtCo/ZrO_2$ catalyze the selective formation of $CH_4$. As $PtCo/CeO_2$ and $PtCo/ZrO_2$ behave similarly (see the Supporting Information), either $PtCo/CeO_2$ or $PtCo/ZrO_2$ was used as a representative system for comparison with $PtCo/TiO_2$.

As $CO_2$ does not adsorb strongly onto single-crystal surfaces under ultrahigh vacuum conditions, $PtCo/TiO_2(110)$ and $PtCo/CeO_2(110)$ model surfaces were analyzed by AP-XPS to identify possible reaction intermediates for $CO_2$ reduction by $H_2$. The surface-species C 1s peaks at 292.8 eV

[*] Dr. S. Kattel,[+] Dr. X. Yang, Dr. B. Yan, Dr. P. Liu, Prof. Dr. J. G. Chen
Chemistry Department, Brookhaven National Laboratory
2 Center St., Upton, NY 11973 (USA)
E-mail: pingliu3@bnl.gov
Dr. W. Yu,[+] W. Wan, Prof. Dr. J. G. Chen
Department of Chemical Engineering
Columbia University
1500 W. 120th St., New York, NY 10027 (USA)
E-mail: jgchen@columbia.edu
Y. Huang
Dalian Institute of Chemical Physics
Chinese Academy of Science
Dalian, 116023 (China)
[+] These authors contributed equally to this work.

Supporting information for this article can be found under: http://dx.doi.org/10.1002/anie.201601661.

  

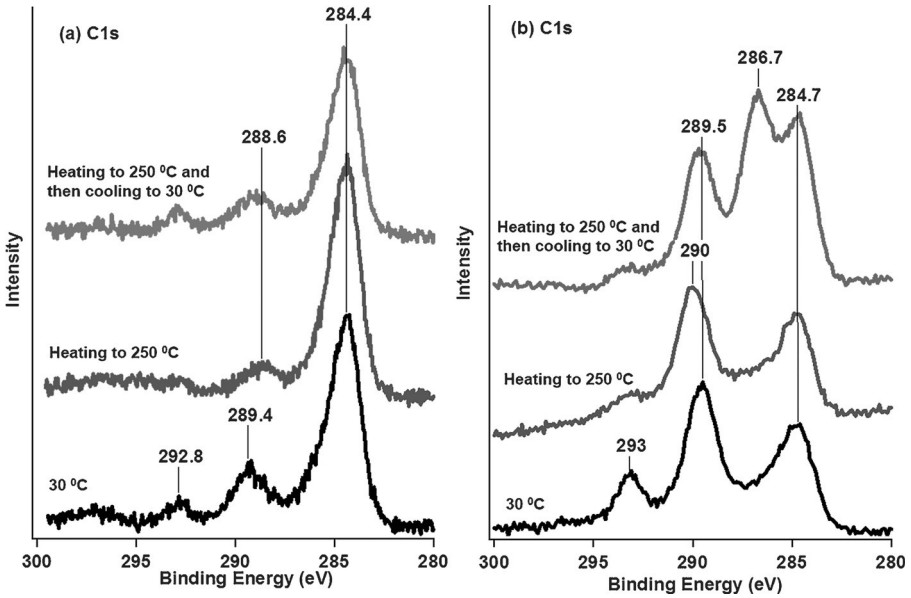


***Figure 1.*** C 1s AP-XPS of a) $PtCo/TiO_2$ and b) $PtCo/CeO_2$ after exposure to $CO_2$ (100 mTorr) and $H_2$ (600 mTorr).

for $PtCo/TiO_2(110)$ (Figure 1a) and 293.0 eV for $PtCo/CeO_2(110)$ (Figure 1b) denote gas-phase $CO_2$. The features at 289.4 eV in Figure 1a and 289.5 eV in Figure 1b are attributed to the formation of carbonate ($*CO_3$) or formate (*HCOO)/carboxyl (*HOCO) species on both surfaces. These surface intermediates have previously been identified by AP-XPS on a $CeO_x/Cu(111)$ surface after exposure to $CO_2$ under ambient pressure.[3d,13] The peaks at approximately 284.4 eV in Figure 1a and 284.7 eV in Figure 1b indicate the presence of carbon on both surfaces. Upon heating to 250 °C and cooling down to room temperature, a peak at approximately 286.7 eV was observed for $PtCo/CeO_2(110)$ but not for $PtCo/TiO_2(110)$. This peak corresponds to the formation of methoxy ($*CH_3O$) species, suggesting that $CO_2$ hydrogenation may follow different reaction pathways on the $PtCo/TiO_2(110)$ and $PtCo/CeO_2(110)$ surfaces (see below).

The TEM results in Table 1 and in the Supporting Information, Figure S1 show that the size distributions for the three catalysts are fairly similar. Furthermore, the formation of Pt–Co bonds was confirmed for all catalysts by EXAFS (Tables 1 and S2 and Figure S2). $CO_2$ hydrogenation was evaluated in a flow reactor at 300 °C, with the activity being presented in terms of both the conversion and the turnover frequency (TOF) by normalizing against the CO uptake for each catalyst. The $CO_2$ conversion over the three catalysts was very similar, indicating that the selectivity can significantly vary while the conversion hardly changes (Table 1). The ratio of $CO/CH_4$ formed over the $PtCo/TiO_2$ catalyst was 85, which is far higher than those for $PtCo/CeO_2$ (12) and $PtCo/ZrO_2$ (8.5), revealing that $PtCo/TiO_2$ selectively produces CO, whereas the other two supports favor the formation of $CH_4$.

***Table 1:*** Particle size, coordination number (CN), CO chemisorption, steady-state $CO_2$ conversion, turnover frequency (TOF), and $CO/CH_4$ ratio for the $PtCo/TiO_2$, $PtCo/CeO_2$, and $PtCo/ZrO_2$ catalysts.

| Catalyst | $PtCo/TiO_2$ | $PtCo/CeO_2$ | $PtCo/ZrO_2$ |
|---|---|---|---|
| particle size [nm] | $2.3\pm0.5$ | $2.7\pm1.0$ | $2.3\pm0.7$ |
| CN (Pt–Pt) | $4.2\pm0.6$ | $5.1\pm1.3$ | $4.3\pm2.1$ |
| CN (Pt–Co) | $1.7\pm0.5$ | $2.7\pm0.6$ | $2.3\pm1.6$ |
| CO chemisorption [$\mu mol\,g^{-1}$] | 18.7 | 36.4 | 39.4 |
| $CO_2$ conversion [%] | 8.2 | 9.1 | 7.8 |
| TOF [$min^{-1}$] | 35.3 | 20.1 | 16.0 |
| $CO/CH_4$ ratio | 85 | 12 | 8.5 |

A batch reactor equipped with an FTIR spectrometer was used to monitor surface intermediates and the gas-phase composition during the reaction. The FTIR spectra recorded after the reaction of $CO_2$ and $H_2$ on $PtCo/CeO_2$ and $PtCo/TiO_2$ powder catalysts (Figure S3) are consistent with the findings from the AP-XPS study on the model surfaces (Figure 1). The bands at 1373 $cm^{-1}$ and 1610 $cm^{-1}$ were assigned to the symmetric and antisymmetric OCO vibrations (Table S3), respectively, of formate-like species, suggesting the presence of both HCOO* and HOCO* surface intermediates on both catalysts. Furthermore, for $PtCo/CeO_2$, vibrational features (bands at 1420 $cm^{-1}$ and 2869 $cm^{-1}$) indicative of the $\delta(CH_3)$ and $\nu_s(CH_3)$ modes (Table S3) in $*CH_3O$[14] were also observed, suggesting the presence of the $*CH_3O$ intermediate.

Various gas-phase reaction products were also identified by their characteristic vibrational modes. The vibrational modes $\nu(C{=}O)$ at 2358 $cm^{-1}$, $\nu(C{\equiv}O)$ at 2170 $cm^{-1}$, and $\nu(C{-}H)$ at 3016 $cm^{-1}$ were used to monitor the presence of $CO_2$, CO, and $CH_4$, respectively. On $PtCo/TiO_2$, aside from a sharp band corresponding to $CO_2$, CO was also detected (Figure 2a). On $PtCo/CeO_2$, vibrational peaks indicative of the formation of $CH_4$ were observed in addition to the characteristic CO band.

The involvement of these surface reaction intermediates was also confirmed by reacting $CH_3OH$ or formic acid (HCOOH) in the batch reactor under the same conditions as for $CO_2$ hydrogenation to monitor and compare the reaction products. As shown in Figure 2b, the reaction products are almost identical for $PtCo/CeO_2$ and $PtCo/TiO_2$. CO and $CO_2$ were produced from both $CH_3OH$ and HCOOH, indicating that *HCOO is a likely reaction intermediate on both $PtCo/CeO_2$ and $PtCo/TiO_2$. $CH_4$ was only produced from $CH_3OH$, suggesting that the surface $*CH_3O$ intermediate is a likely precursor for the formation of $CH_4$. However, the conversion of $CH_3OH$ into $CH_4$ occurred on both surfaces. Accordingly, the role that the $TiO_2$ support plays in preventing the formation of $*CH_3O$ and therefore $CH_4$ on $PtCo/TiO_2$ must be related to the steps before $*CH_3O$ formation.

  

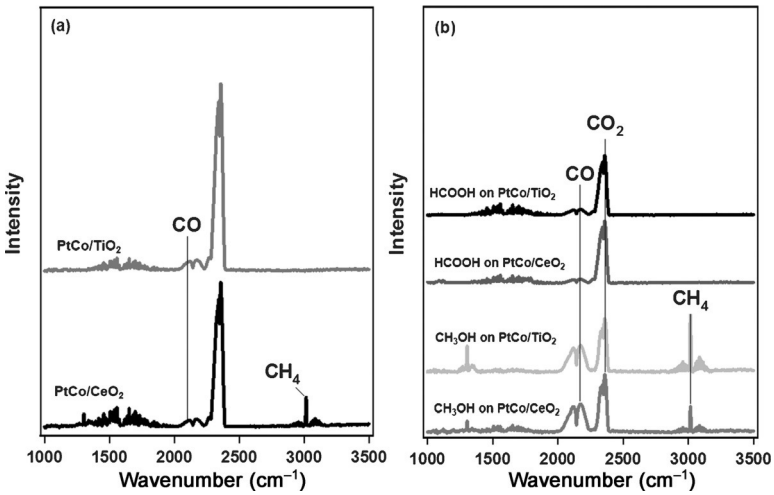


***Figure 2.*** FTIR spectra recorded during a) $CO_2$ reduction in the presence of $H_2$ and b) the reactions of formic acid and methanol over $PtCo/CeO_2$ and $PtCo/TiO_2$ catalysts.

Overall, the experimental results with $CeO_2$ and $TiO_2$ supported PtCo powder catalysts indicate that different reaction intermediates lead to the different $CO/CH_4$ selectivities in the flow reactor. The $CO/CH_4$ selectivity is much greater over $PtCo/TiO_2$ than over $PtCo/CeO_2$ (Table 1). On $PtCo/TiO_2$, *HCOO is formed as an intermediate, which may eventually produce CO. On $PtCo/CeO_2$, aside from the route that proceeds via *HCOO, a pathway via a $*CH_3O$ intermediate is operating in parallel, which likely leads to the formation of $CH_4$. Yet, at this stage, it is still unclear how the oxide supports tune the selectivity, and a better understanding of the detailed reaction network and the active sites is required, which is extremely difficult to obtain using only experimental techniques. Therefore, DFT calculations were carried out to determine the mechanism of $CO_2$ hydrogenation at the metal–oxide interfaces.

Pt-terminated surface structures have been predicted by DFT as the thermodynamically most stable structures and detected in surface experiments over model Co/Pt(111) surfaces[15] and Co/Pt thin films[16] for clean surfaces and in the presence of hydrogen. Figure S4 shows the DRIFTS measurements of CO adsorption over supported $PtCo/ZrO_2$. The relatively intense vibrational peaks of linearly adsorbed CO on the bimetallic $PtCo/ZrO_2$ catalyst are much more similar to those of $Pt/ZrO_2$ than those of $Co/ZrO_2$, which is consistent with a Pt-terminated bimetallic surface. The PtCo–oxide interface was modeled by depositing a small oxide cluster on the PtCo(111) support, where a $Pt_{1ML}/Co_{1ML}$/Pt(111) near-surface model was used, and the hydroxylation of oxides in hydrogen-rich environments was also considered (Figure 3). Such an inverse model has previously been shown to be a reasonable system for describing the catalytic properties of metal–oxide catalysts under $CO_2$ hydrogenation conditions.[3d,8a,17] Owing to the deficiencies of standard DFT calculations in describing $CeO_x$, as discussed in more detail in the Supporting Information,[18] $PtCo/TiO_2$ and $PtCo/ZrO_2$ were used as representative catalysts for the selective formation of CO and $CH_4$, respectively, in our theoretical study.

The reaction network for $CO_2$ hydrogenation typically includes a pathway based on a reverse water–gas shift (RWGS) followed by CO hydrogenation (Figure S5) and the formate pathway.[19] Our results show that the binding geometries of the reaction intermediates are similar on both $PtCo/TiO_2$ and $PtCo/ZrO_2$ (Figures S6 and S7). In general, C-bound species prefer Pt sites with an $\eta^1$-$C_{Pt}$ bonding mode, whereas O-bound species prefer to bind to reduced $M^{\delta+}$ cations in the metal oxides with $\eta^1$-$O_M{}^{\delta+}$ configuration. For species bound through both C and O (C,O-bound species; for example, $*CO_2$, *HOCO, *CO, *CHO, *CHOH, $*CH_2O$, and $*CH_2OH$), the metal–oxide interfacial sites are favored with $\eta^2$-$C_{Pt}O_M{}^{\delta+}$ configuration. Thus the metal–oxide interface is likely to play an important role in activating chemically inert $CO_2$ and facilitating its subsequent conversion.[3d,8a]

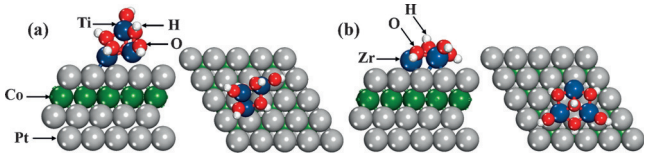


***Figure 3.*** Side and top views of the DFT-optimized structures for model hydroxylated $Ti_3O_6/PtCo(111)$ (a) and $Zr_3O_6/PtCo(111)$ (b) surfaces.

CO and $CH_4$ production on $PtCo/TiO_2$ preferentially proceeds through RWGS and CO hydrogenation (Figure 4a). The adsorption of $CO_2$ leads to the formation of a carboxylate ($CO_2{}^{\delta-}$) that is strongly bound at the PtCo–$TiO_2$ interface as a bent O–C–O motif in an $\eta^2$-$C_{Pt}O_{Ti}{}^{\delta+}$ configuration (Figure S5b). Such a binding motif favors the hydrogenation to *HOCO (Figure S5c) with a reaction energy ($\Delta E$) of −0.56 eV and a small activation energy ($E_a$) of 0.23 eV, as the transition only involves one O–H bond formation with a small distortion in the geometry of $*CO_2$. In contrast, $*CO_2$ hydrogenation to *HCOO is kinetically and thermodynamically less favorable ($\Delta E = -0.25$ eV, $E_a = 0.51$ eV). The produced *HOCO then dissociates into *CO and *OH ($\Delta E = -0.26$ eV, $E_a = 0.93$ eV), and *OH is hydrogenated to form $*H_2O$ ($E_a = 0.43$ eV) while *CO either desorbs or undergoes further hydrogenation reactions. The hydrogenation of *CO to *CHO is exothermic by only −0.05 eV. The corresponding $E_a$ (1.40 eV) is comparable to the BE of CO (−1.51 eV; see Table S4). However, under the reaction conditions, the entropy contribution significantly lowers the barrier for *CO desorption by 1.28 eV at 300 °C, and the desorption barrier is much lower than that for the hydrogenation to *CHO. Thus, corroborating our experimental finding (Table 1), the DFT results show that CO(g) is the main product of $CO_2$ hydrogenation over $PtCo/TiO_2$.

The minor side products result from the *CHO intermediate, which can be hydrogenated to either $*CH_2O$ or

  

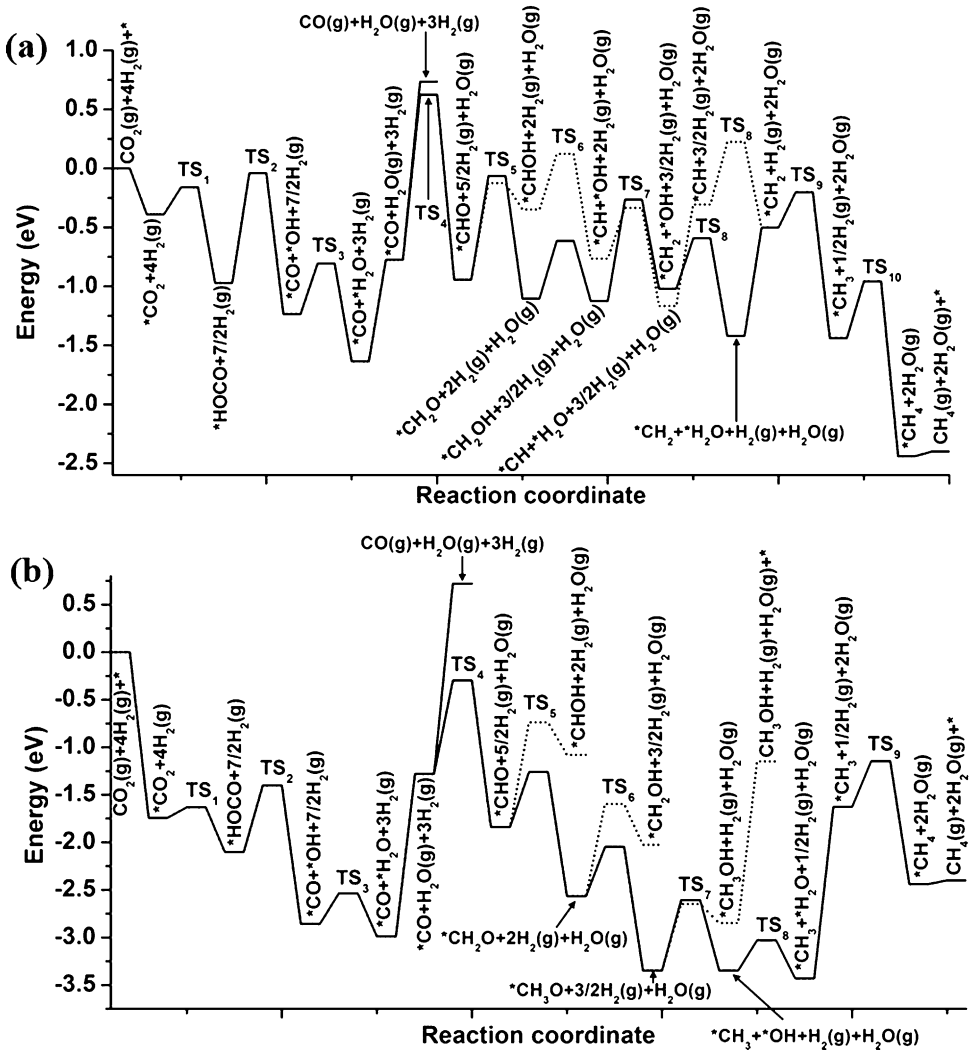


***Figure 4.*** Potential energy diagrams for the synthesis of CO and $CH_4$ through the RWGS and CO hydrogenation pathway on model hydroxylated $Ti_3O_6$/PtCo(111) (a) and $Zr_3O_6$/PtCo(111) (b) surfaces.

*CHOH. Figure 4a shows that the two steps are competitive with a difference in $E_a$ of only 0.06 eV (0.82 eV vs. 0.88 eV). *CHOH is the precursor for C–O bond cleavage to form *CH and *OH ($\Delta E = -0.42$ eV, $E_a = 0.47$ eV). *CH then undergoes three exothermic hydrogenation reactions to form $CH_4$, where the highest barrier is calculated for $*H + *CH_3 \rightarrow *CH_4 + *$ ($E_a = 0.48$ eV). The produced $*CH_2O$ is further hydrogenated to form $*CH_2OH$ ($E_a = 0.49$ eV), which dissociates into $*CH_2$ and *OH ($\Delta E = 0.10$ eV and $E_a = 0.86$ eV), eventually leading to $*CH_4$ production. The formation of $*CH_3O$ ($E_a = 0.60$ eV) is less favorable. The DFT results agree well with the experiments on the PtCo/$TiO_2$ model and powder catalysts, where the $*CH_3O$ intermediate and therefore $CH_3OH$(g) are not observed during $CO_2$ hydrogenation. Therefore, the minor side product for $CO_2$ hydrogenation over PtCo/$TiO_2$ is $CH_4$(g), which is consistent with the experimental results (Table 1).

For comparison, on PtCo/$ZrO_2$, the binding of C,O-bound and O-bound species at the interface is selectively strengthened as $O{-}Zr^{\delta+}$ bonds are formed (Table S4 and Figure S7), whereas for the C-bound species, the BEs of the Pt–C interactions are the same as for $TiO_2$/PtCo(111). According to the calculated partial density of states (PDOS, Figure S8), the promoted $O{-}Zr^{\delta}$ interaction is associated with an increased density of states near the Fermi level compared to $Ti^{\delta+}$. Thus, although the $CO_2$ hydrogenation follows the same pathway in both cases, differences in the reaction and activation energies are clearly observed (Figure 4b). On PtCo/$ZrO_2$, $*CO_2$ hydrogenation to *HOCO ($\Delta E = -0.39$ eV, $E_a = 0.11$ eV), *HOCO dissociation to *CO and *OH ($\Delta E = -0.75$ eV, $E_a = 0.70$ eV), as well as *CO hydrogenation to *CHO ($\Delta E = -0.48$ eV, $E_a = 0.98$ eV) are energetically more favorable; in contrast, *CO desorption is more difficult owing to the stronger CO BE (−2.00 eV). In this case, even when including entropy contributions, the energy required for *CO hydrogenation is comparable with that necessary for *CO desorption. Therefore, CO is only formed as a minor product over PtCo/$ZrO_2$ whereas the major products should result from *CO hydrogenation, such as $CH_4$ and/or $CH_3OH$.

Furthermore, *CHO on the PtCo/$ZrO_2$ interface is preferentially hydrogenated to $*CH_2O$ ($\Delta E = -0.74$ eV, $E_a = 0.58$ eV) rather than *CHOH ($\Delta E = 0.76$ eV, $E_a = 1.10$ eV; Figure 4b). The sequential hydrogenation of $*CH_2O$ results in $*CH_3O$ formation ($\Delta E = -0.72$ eV, $E_a = 0.52$ eV) in contrast to the endothermic formation of $*CH_2OH$ ($\Delta E = 0.54$ eV, $E_a = 0.97$ eV). This is in good agreement with the experimental detection of the $*CH_3O$ intermediate on the PtCo/$ZrO_2$ model surface (Figure 1) and powder catalyst (Figure S3). Hydrogenation of $*CH_3O$ to give $*CH_3OH$ ($\Delta E = 0.50$ eV, $E_a = 0.70$ eV) or $*CH_3$ and *OH ($\Delta E = 0.01$ eV, $E_a = 0.74$ eV) is likely to be competitive; however, owing to the favorable binding at the PtCo–$ZrO_2$ interface, desorption of $*CH_3OH$ is uphill in energy by 1.72 eV. Furthermore, the formed $*CH_3OH$ is not stable and prefers dissociation to $*CH_3O$ ($E_a = 0.20$ eV) over desorption ($E_a = 1.72$ eV). In contrast, $*CH_3$ hydrogenation to $*CH_4$ is much easier ($\Delta E = -0.95$, $E_a = 0.48$ eV). Therefore, as observed experimentally (Table 1), the DFT calculations predict that $CH_4$ is the major product resulting from the hydrogenation of *CO on PtCo/$ZrO_2$. Finally, the most

  

difficult step, and likely the activity-controlling step, along the reaction pathway (Figure 4) varies from *HOCO dissociation on $PtCo/TiO_2$ to *CO hydrogenation to *HCO on $PtCo/ZrO_2$; however, the corresponding barriers are similar (0.93 eV vs. 0.98 eV). Accordingly, only a small decrease in TOF is expected, which agrees well with our measurements (Table 1).

In summary, our experimental and theoretical investigations have shown that by changing the oxide support from $TiO_2$ to $CeO_2$ or $ZrO_2$, the selectivity of bimetallic PtCo catalysts in $CO_2$ hydrogenation can be tuned while the overall activity is hardly affected. $CeO_2$ or $ZrO_2$ supported PtCo catalysts display high selectivity towards $CH_4$, whereas CO is preferentially formed with a $TiO_2$ support. According to an AP-XPS analysis of model surfaces and the FTIR spectra of the powder catalysts, the difference in selectivity is likely associated with different dominant reaction pathways. *HCOO/*HOCO are observed as reaction intermediates on $PtCo/TiO_2$ whereas both *HCOO/*HOCO and $*CH_3O$ are observed on $PtCo/CeO_2$ and $PtCo/ZrO_2$. The DFT study well describes the experimental observations and indicates that the metal–oxide interface promotes the heterogeneity of the active sites. Unlike the binding of C-bound species, the binding of C,O-bound and O-bound species is tuned selectively at the interface. Changing the support from $TiO_2$ to $ZrO_2$ does not affect the dominant RWGS and CO hydrogenation pathway; however, CO formation is hindered, and $CH_4$ is preferentially formed over $ZrO_2$. The synergy between the metal and oxide at the metal–oxide interface thus plays an important role in tuning the selectivity of $CO_2$ hydrogenation reactions over oxide-supported PtCo bimetallic catalysts.

## Experimental Section

The catalysts were prepared by the incipient wetness impregnation method with an aqueous solution of the respective metal precursors ($(NH_3)_4Pt(NO_3)_2$ and $Co(NO_3)_2{\cdot}6H_2O$ from Alfa Aesar). The metal loadings (wt%) of the PtCo bimetallic catalysts were 1.7% Pt and 1.5% Co. After impregnation, the samples were dried at 60°C overnight and calcined in air at 290°C for 2 h. The PtCo bimetallic catalyst was selected because it led to higher $CO_2$ conversion than the corresponding monometallic catalysts.[3e]

The DFT calculations were performed using the Vienna Ab Initio Simulation Package (VASP) code.[20] Electron–ion interactions were treated by the projector-augmented wave (PAW) method. The exchange and correlation energies were described using the generalized gradient approximation with the Perdew–Wang (PW91) functional. A cutoff energy of 400 eV and a $3\times3\times1$ Monkhorst–Pack k point grid were used. For further details of the theoretical models and the synthesis/characterization methods, see the Supporting Information.

## Acknowledgements

This material is based upon work supported by the U.S. Department of Energy, Office of Science (Contract No. DE-SC0012704). The DFT calculations were performed using computational resources at the Center for Functional Nanomaterials, a user facility at BNL, supported by the US Department of Energy and the National Energy Research Scientific Computing Center (NERSC), which is supported by the Office of Science of the U.S. Department of Energy (DE-AC02-05CH11231).

**Keywords:** bimetallic catalysts · carbon dioxide · heterogeneous catalysis · hydrogenation · supported catalysts

**How to cite:** *Angew. Chem. Int. Ed.* **2016**, *55*, 7968–7973
*Angew. Chem.* **2016**, *128*, 8100–8105

[1] P. Sabatier, *La catalyse en chimie organique*, Librairie Polytechnique, Paris et Liège, **1920**.
[2] a) F. Calle-Vallejo, J. Tymoczko, V. Colic, Q. H. Vu, M. D. Pohl, K. Morgenstern, D. Loffreda, P. Sautet, W. Schuhmann, A. S. Bandarenka, *Science* **2015**, *350*, 185–189; b) J. K. Nørskov, T. Bligaard, J. Rossmeisl, C. H. Christensen, *Nat. Chem.* **2009**, *1*, 37–46.
[3] a) D. J. Stacchiola, S. D. Senanayake, P. Liu, J. A. Rodriguez, *Chem. Rev.* **2013**, *113*, 4373–4390; b) E. A. Monyoncho, S. Ntais, N. Brazeau, J.-J. Wu, C.-L. Sun, E. A. Baranova, *ChemElectroChem* **2016**, *3*, 218–227; c) G. R. Jenness, J. R. Schmidt, *ACS Catal.* **2013**, *3*, 2881–2890; d) J. Graciani, K. Mudiyanselage, F. Xu, A. E. Baber, J. Evans, S. D. Senanayake, D. J. Stacchiola, P. Liu, J. Hrbek, J. F. Sanz, J. A. Rodriguez, *Science* **2014**, *345*, 546–550; e) M. D. Porosoff, J. G. G. Chen, *J. Catal.* **2013**, *301*, 30–37; f) Y. Hartadi, D. Widmann, R. J. Behm, *ChemSusChem* **2015**, *8*, 456–465.
[4] a) K. Mudiyanselage, S. D. Senanayake, L. Feria, S. Kundu, A. E. Baber, J. Graciani, A. B. Vidal, S. Agnoli, J. Evans, R. Chang, S. Axnanda, Z. Liu, J. F. Sanz, P. Liu, J. A. Rodriguez, D. J. Stacchiola, *Angew. Chem. Int. Ed.* **2013**, *52*, 5101–5105; *Angew. Chem.* **2013**, *125*, 5205–5209; b) A. Bruix, J. A. Rodriguez, P. J. Ramírez, S. D. Senanayake, J. Evans, J. B. Park, D. Stacchiola, P. Liu, J. Hrbek, F. Illas, *J. Am. Chem. Soc.* **2012**, *134*, 8968–8974; c) F. Calaza, C. Stiehler, Y. Fujimori, M. Sterrer, S. Beeg, M. Ruiz-Oses, N. Nilius, M. Heyde, T. Parviainen, K. Honkala, H. Häkkinen, H.-J. Freund, *Angew. Chem. Int. Ed.* **2015**, *54*, 12484–12487; *Angew. Chem.* **2015**, *127*, 12661–12665; d) J. Y. Park, L. R. Baker, G. A. Somorjai, *Chem. Rev.* **2015**, *115*, 2781–2817.
[5] J. Saavedra, H. A. Doan, C. J. Pursell, L. C. Grabow, B. D. Chandler, *Science* **2014**, *345*, 1599–1602.
[6] a) M. G. Willinger, W. Zhang, O. Bondarchuk, S. Shaikhutdinov, H.-J. Freund, R. Schlögl, *Angew. Chem. Int. Ed.* **2014**, *53*, 5998–6001; *Angew. Chem.* **2014**, *126*, 6108–6112; b) L. Yu, Y. Liu, F. Yang, J. Evans, J. A. Rodriguez, P. Liu, *J. Phys. Chem. C* **2015**, *119*, 16614–16622; c) J. C. Matsubu, V. N. Yang, P. Christopher, *J. Am. Chem. Soc.* **2015**, *137*, 3076–3084.
[7] a) M. A. A. Aziz, A. A. Jalil, S. Triwahyono, A. Ahmad, *Green Chem.* **2015**, *17*, 2647–2663; b) G. Melaet, W. T. Ralston, C.-S. Li, S. Alayoglu, K. An, N. Musselwhite, B. Kalkan, G. A. Somorjai, *J. Am. Chem. Soc.* **2014**, *136*, 2260–2263.
[8] a) X. F. Yang, S. Kattel, S. D. Senanayake, J. A. Boscoboinik, X. W. Nie, J. Graciani, J. A. Rodriguez, P. Liu, D. J. Stacchiola, J. G. G. Chen, *J. Am. Chem. Soc.* **2015**, *137*, 10104–10107; b) C. Liu, B. Yang, E. Tyo, S. Seifert, J. DeBartolo, B. von Issendorff, P. Zapol, S. Vajda, L. A. Curtiss, *J. Am. Chem. Soc.* **2015**, *137*, 8676–8679.
[9] a) M. D. Porosoff, X. F. Yang, J. A. Boscoboinik, J. G. Chen, *Angew. Chem. Int. Ed.* **2014**, *53*, 6705–6709; *Angew. Chem.* **2014**, *126*, 6823–6827; b) H.-K. Lim, H. Shin, W. A. Goddard, Y. J. Hwang, B. K. Min, H. Kim, *J. Am. Chem. Soc.* **2014**, *136*, 11355–11361; c) C. Costentin, S. Drouet, M. Robert, J.-M. Savéant, *Science* **2012**, *338*, 90–94.
[10] W.-H. Cheng, *Acc. Chem. Res.* **1999**, *32*, 685–691.
[11] a) L. C. Grabow, M. Mavrikakis, *ACS Catal.* **2011**, *1*, 365–384; b) Y. Yang, J. Evans, J. A. Rodriguez, M. G. White, P. Liu, *Phys. Chem. Chem. Phys.* **2010**, *12*, 9909–9917.

  

[12] a) W. L. Zhu, Y. J. Zhang, H. Y. Zhang, H. F. Lv, Q. Li, R. Michalsky, A. A. Peterson, S. H. Sun, *J. Am. Chem. Soc.* **2014**, *136*, 16132 – 16135; b) Q. Lu, J. Rosen, Y. Zhou, G. S. Hutchings, Y. C. Kimmel, J. G. G. Chen, F. Jiao, *Nat. Commun.* **2014**, *5*, 3242; c) S. Back, M. S. Yeom, Y. Jung, *ACS Catal.* **2015**, *5*, 5089 – 5096.
[13] X. Deng, A. Verdaguer, T. Herranz, C. Weis, H. Bluhm, M. Salmeron, *Langmuir* **2008**, *24*, 9474 – 9478.
[14] T. G. Kelly, A. L. Stottlemyer, H. Ren, J. G. Chen, *J. Phys. Chem. C* **2011**, *115*, 6644 – 6650.
[15] C. A. Menning, H. H. Hwu, J. G. Chen, *J. Phys. Chem. B* **2006**, *110*, 15471 – 15477.
[16] C. A. Menning, J. G. Chen, *J. Power Sources* **2010**, *195*, 3140 – 3144.
[17] T. Lunkenbein, J. Schumann, M. Behrens, R. Schlögl, M. G. Willinger, *Angew. Chem. Int. Ed.* **2015**, *54*, 4544 – 4548; *Angew. Chem.* **2015**, *127*, 4627 – 4631.
[18] D. Lu, P. Liu, *J. Chem. Phys.* **2014**, *140*, 084101.
[19] P. Liu, Y. Yang, M. G. White, *Surf. Sci. Rep.* **2013**, *68*, 233 – 272.
[20] a) G. Kresse, J. Furthmüller, *Comp. Mater. Sci.* **1996**, *6*, 15 – 50; b) G. Kresse, J. Furthmüller, *Phys. Rev. B* **1996**, *54*, 11169 – 11186.

Received: February 16, 2016
Revised: April 13, 2016
Published online: May 9, 2016

  